Self-similar formation of an inverse cascade in vibrating elastic plates

Gustavo Düring,[1] Christophe Josserand,[2] and Sergio Rica[3]

[1]*Facultad de Física, Pontificia Universidad Católica de Chile, Casilla 306, Santiago, Chile*

[2]*Sorbonne Universités, CNRS & UPMC Univ Paris 06, UMR 7190, Institut d'Alembert, F-75005, Paris, France*

[3]*Facultad de Ingeniería y Ciencias, Universidad Adolfo Ibáñez, Avda. Diagonal las Torres 2640, Peñalolén, Santiago, Chile*

The dynamics of random weakly nonlinear waves is studied in the framework of vibrating thin elastic plates. Although it has been previously predicted that no stationary inverse cascade of constant wave action flux could exist in the framework of wave turbulence for elastic plates, we present substantial evidence of the existence of a time-dependent inverse cascade, opening up the possibility of self-organization for a larger class of systems. This inverse cascade transports the spectral density of the amplitude of the waves from short up to large scales, increasing the distribution of long waves despite the short-wave fluctuations. This dynamics appears to be self-similar and possesses a power-law behavior in the short-wavelength limit which significantly differs from the exponent obtained via a Kolmogorov dimensional analysis argument. Finally, we show explicitly a tendency to build a long-wave coherent structure in finite time.

I. INTRODUCTION

Oscillating random waves are present in a myriad of situations in nature, displaying a large variety of scales and exhibiting turbulent-like behavior, so-called wave turbulence [1–3]. Of particular interest are the oscillations over the surface of the sea, Rossby waves in atmospherical science, nonlinear optics, plasma oscillations, and the vibration of elastic bodies such as piano strings, timbals, or more complex singing bowls, bells, or gongs. Because of the intrinsic nonlinearity of the basic underlying physics of these problems, and because of the randomness of the phase of the oscillations, only a statistical description seems reasonable. The weak turbulence theory provides such a statistical description for the asymptotic long-time behavior of the spectral wave amplitude, in the case where nonlinearities are small. In particular, it describes the energy transfer among the different modes in agreement with the conservation of the total energy of the waves. More precisely, this wave turbulence theory provides kinetic equations for the long-time evolution of the spectral amplitude for dispersive wave systems [1–3]. In the present context of small nonlinearities, we will use interchangeably wave turbulence theory and weak turbulence theory and refer to it as WTT. Remarkably, such kinetic equations exhibit stationary solutions corresponding to equipartition or constant flux cascades of the energy, namely the Rayleigh-Jeans solution and the Kolmogorov-Zakharov (KZ) spectrum, respectively. The search of the KZ spectra has motivated exhaustive studies since the early 1960s [3], regaining recent interest, because of the parallel development of new theoretical and experimental findings. Among them, we mention the cases of surface capillary waves [4,5], surface gravity waves [6,7], and elastic waves of thin plates [8–10], for instance. While such dynamics corresponds usually to a direct cascade of energy towards the small scales, the formation of large-scale structure can sometimes be observed. This is the case in particular for Bose-Eintein condensation [11–14] or in two-dimensional hydrodynamic turbulence [15], where the self-organization process is a consequence of an inverse cascade. This inverse cascade transfers some quantity (e.g., particles, enstrophy, and wave action) from the small scales toward the large scales

leading to the formation of coherent structures. The formation of an inverse cascade in different systems has always been related to the existence of a conserved quantity at least at the weakly nonlinear level. For instance, when using the Gross-Pitaevskii or nonlinear Schrödinger equation to model the Bose-Einstein condensates, WTT predicts the existence of an inverse cascade of mass (a conserved quantity). Similarly, in the case of surface gravity waves, an inverse cascade of the conserved wave action is deduced and numerically observed [16,17]. Finally, we want to emphasize that, besides the description of the stationary solutions of the dynamics, the kinetic equations that are deduced by the WTT give a very good framework to investigate nonstationary situations involved in wave systems such as transitory or decaying regimes that often lead to self-similar dynamics [18–20]. The goal of this paper is to show, using the elastic vibrating plate, that the formation of an inverse cascade does not generally require a conserved quantity, opening up the possibility of self-organization for a larger class of systems. In particular, nothing prevents the existence of a time-dependent inverse cascade that would transfer wave action from short scale to large scale.

The paper is organized as follows: Section II introduces the dynamical version of the Föppl–von Kármán equations which provide the basic nonlinear equations for vibrating elastic plates, containing both bending and stretching. Then we summarize the main findings of the WTT of a vibrating plate, in particular the concept of the Kolmogorov-Zakharov spectra. Section III presents the numerical simulations of a vibrating plate which is forced only at very short wavelengths, displaying a striking inverse cascade of wave action. Section IV analyzes the numerical evidence of a self-similar evolution which suggests a blow-up in finite time. Finally, we conclude with an overall discussion of the problem.

II. WAVE TURBULENCE THEORY OF VIBRATING ELASTIC PLATES

A. The Föppl–von Kármán equations for elastic plates

Vibrating elastic plates offer, perhaps, the most suitable weakly nonlinear wave system. It is studied within the

framework of the dynamical version of the Föppl–von Kármán equations [21] which model the dynamics of the out-of-plane displacements of the plate. We shall use the same notations as in Ref. [8], but we write them in dimensionless units. We choose $l = h/\sqrt{3(1 - \sigma^2)}$ as the unit of length and $l\sqrt{\frac{\rho}{E}}$ as the unit of time. Here h is the thickness of the elastic sheet, the material has a mass density ρ, a Young modulus E, and its Poisson ratio is σ. In these units the equations read:

$$\frac{\partial^2 \zeta}{\partial t^2} = -\frac{1}{4}\Delta^2 \zeta + \{\zeta, \chi\}, \qquad (1)$$

$$\Delta^2 \chi = -\frac{1}{2}\{\zeta, \zeta\}. \qquad (2)$$

The out-of-plane displacement of the plate in physical units is thus $l\zeta(x, y, t)$, and the Airy stress function is $El^2\chi(x, y, t)$. Equation (2) for the Airy stress function $\chi(x, y, t)$ may be seen as the compatibility equation for the in-plane stress tensor which follows the dynamics at the lowest order.[1] The characteristic size of the plate is L, thus the dynamics of a free plate is governed by a single dimensionless parameter, $\Lambda = \frac{L}{l} = \sqrt{3(1 - \sigma^2)}\frac{L}{h}$, which is typically of the order of 10^3 up to 10^4. $\Delta = \partial_{xx} + \partial_{yy}$ is the usual Laplacian and the bracket $\{\cdot, \cdot\}$ is defined by $\{f, g\} \equiv f_{xx}g_{yy} + f_{yy}g_{xx} - 2f_{xy}g_{xy}$, which is an exact divergence, so Eq. (1) preserves the momentum of the center of mass, hence, $\partial_{tt}\int \zeta(x, y, t)\, dx\, dy = 0$. Moreover, the total energy:

$$E = \int \left[\frac{1}{2}(\partial_t \zeta)^2 + \frac{1}{8}(\Delta \zeta)^2 - \frac{1}{2}(\Delta \chi)^2 - \frac{1}{2}\chi\{\zeta, \zeta\}\right] dx\, dy \qquad (3)$$

is also conserved by the dynamics (1) and (2). Finally, small plane-wave perturbations [$\zeta \sim e^{i(k \cdot x - \omega_k t)}$ with $x = (x, y)$] of a plane plate are dispersive with the usual ballistic behavior of bending waves, that is, $\omega_k = \frac{1}{2}|k|^2$ [21].

B. Wave turbulence equations for the spectral densities

As already discussed in Ref. [8], Eqs. (1) and (2) exhibit a Hamiltonian structure which is easily revealed in Fourier space, defined by $\zeta_k(t) = \frac{1}{2\pi}\int \zeta(x, t)e^{ik \cdot x}d^2x$, with $\zeta_k = \zeta^*_{-k}$. The Hamiltonian structure allows one to performs a canonical transformation,

$$\zeta_k = \frac{1}{\sqrt{2\omega_k}}(A_k + A^*_{-k}), \qquad (4)$$

which leads to a diagonalized form of the wave equation:

$$\frac{dA_k}{dt} + i\omega_k A_k = iN_3(A_k), \qquad (5)$$

where $N_3(\cdot)$ abbreviates the cubic nonlinear interaction term given explicitly in Ref. [8].

The WTT describes the long-time statistical behavior of weakly nonlinear random waves. The analysis is based on

_____

[1] In the derivation we have omitted the inertia of the in-plane modes of oscillations, or, in other words, we assume that the in-plane displacements are negligible and the static equilibrium holds, so, as noted, equation (2) describes the dynamics.

an infinite hierarchy of integrodifferential equations for the cumulants of the canonical variables which maybe deduced directly from (5). In the weak wave amplitude limit, a multiscale asymptotic expansion of these hierarchy of equations provides a rational scheme for solving every cumulant [1–3]. As a result, the second-order cumulant,

$$\langle A_{k_1} A^*_{k_2}\rangle = n_{k_1}\delta^{(2)}(k_1 + k_2), \qquad (6)$$

is shown to control the long-time dynamics of the wave system, where n_k is the spectrum of the wave. Other second-order cumulants vanish in the weak amplitude (long-time) limit [1–3], in particular,

$$\langle A_{k_1} A_{k_2}\rangle \to 0 \quad \text{and} \quad \langle A^*_{k_1} A^*_{k_2}\rangle \to 0.$$

In these formulas $\langle \ldots \rangle$ stands for the ensemble average over an underlying joint probability distribution function [2].

The asymptotic perturbation scheme of this theory provides at first order a nonlinear frequency shift to the linear waves, leading to an effective oscillation frequency $\omega_k^{\text{eff}} = \omega_k + \omega_k^{(1)} + \ldots$. This correction due to weak nonlinear effects is a function of the mean spectral density $n_k(t)$ (6) and it reads (in the dimensionless units) [22]:

$$\omega_k^{(1)} = \frac{\pi}{2}\left[\int_0^k \frac{q^2}{k^2}n_q\, q\, dq + \int_k^\infty \frac{k^2}{q^2}n_q\, q\, dq\right]. \qquad (7)$$

Notice that this frequency correction was also obtained by considering a limited number of nonlinear interactions [23]. In addition, in the WWT this frequency shift (7) is useful to quantify the nonlinear effects and, by consequence, the validity of the WTT. Indeed, the ratio $\omega_k^{(1)}/\omega_k$ indicates the relative importance of the nonlinear term with respect to the linear behavior. The uniform validity of the WTT requires that this ratio should satisfy $|\omega_k^{(1)}/\omega_k| \ll 1$ for all the wave numbers. If this number is of the order of unity, wave turbulence is no longer valid, at least for the concerned scales.

At the next order, WTT provides a kinetic equation that governs the mean spectral density evolution $n_k(t)$, which reads [8]:

$$\frac{d}{dt}n_k = \mathcal{C}[n_k] = 12\pi \int dk_1 dk_2 dk_3 \, |J_{-k, k_1; k_2, k_3}|^2$$

$$\times \sum_{s_1 s_2 s_3} n_{k_1} n_{k_2} n_{k_3} n_k \left(\frac{1}{n_k} - \frac{s_1}{n_{k_1}} - \frac{s_2}{n_{k_2}} - \frac{s_3}{n_{k_3}}\right)$$

$$\times \delta^{(2)}(k - k_1 - k_2 - k_3)$$

$$\times \delta\left(\omega_k - s_1\omega_{k_1} - s_2\omega_{k_2} - s_3\omega_{k_3}\right). \qquad (8)$$

The coefficient $J_{-k, k_1; k_2, k_3}$, in Eq. (8), comes from the fourth-order nonlinearities in the total energy (3), and they are given explicitly in Ref. [8]. The details of this scattering function J are not needed here and we do no write it for the sake of simplicity, but, for the purpose of this work, we only have to notice that it has a zero degree of homogeneity in k, that is,

$$J_{-\lambda k, \lambda k_1; \lambda k_2, \lambda k_3} = J_{-k, k_1; k_2, k_3}.$$

Finally, we mention that this function J_{-k, k_1, k_2, k_3} vanishes as $k \to 0$, so the spectrum does not vary at $k = 0$, in agreement

with the original plate equations (1) and (2). If $n_{k=0} = 0$ at $t = 0$, then the spectrum vanishes at $k = 0$ for all time.

The spectral dynamic described by the kinetic equation (8) corresponds to four-wave resonances which enforce the energy and momentum conservations in each interaction. However, in contrast with the case of diluted gases where each collision preserves the number of particles, the total number of waves involved in the interaction is not formally conserved for vibrating plates. Moreover, it is interesting to notice that while the total energy (3) is conserved by the original Föppl–von Kármán equations (1) and (2), the kinetic equation preserves only the quadratic part of the total energy, namely $E_2 = \int [\frac{1}{2}(\partial_t \zeta)^2 + \frac{1}{8}(\Delta \zeta)^2] dx dy$.

The sum in (8) rules for $s_i = \pm 1$, that is, the kinetic equation (8) contains eight terms. Among them, the one corresponding to all s_i equal is not resonant and it thus vanishes. Three other terms (all identical by symmetries) correspond to interactions of two waves coming in and two waves going out, so the total number of waves is preserved by this interaction. We will refer to these terms as the $2 \leftrightarrow 2$ resonant case. Finally, there are four other interaction terms corresponding to one (three) wave(s) coming in and three (one) waves going out, which are referred to as the $3 \leftrightarrow 1$ resonant case. In this latter case, the total number of waves is not preserved formally by the four-wave interaction. We denote these two different interaction terms by $\mathcal{C}_{22}$ and $\mathcal{C}_{13}$, respectively, so $\mathcal{C}[n_k] = \mathcal{C}_{22}[n_k] + \mathcal{C}_{13}[n_k]$. This non wave action conservation represents a major difference with most of the known four-wave interaction systems such as surface gravity waves [24] or nonlinear optics [25]. To our knowledge the only known physical systems that exhibit these two kind of interactions ($2 \leftrightarrow 2$ and $3 \leftrightarrow 1$) are the symmetric capillary waves at the interface between two fluids [5] and the elastic plates [8].

In conclusion, although the kinetic energy $\mathcal{E} = \int \omega_k n_k(t) d^2 k$ is preserved by the dynamics (8), the wave action, $\mathcal{N} = \int n_k(t) d^2 k$, is not.

C. Kolmogorov-Zakharov spectra

Although the wave action is not preserved by the dynamics, local conservation equations can be deduced from the kinetic equation. Indeed, the change in time of the energy spectral density $E(k) = 2\pi k \omega_k n_k$ can be written, after (8), as

$$\frac{d}{dt} E(k) = -\frac{d}{dk} P(k) \quad \text{where}$$

$$P(k) = 2\pi \int_k^\infty \omega_q \mathcal{C}[n_q] q \, dq \tag{9}$$

is the energy flux, which depends, in principle, explicitly on the wave number k and t. Similarly, the wave action flux $Q(k)$ may be defined via the wave action spectral density: $N(k) = 2\pi k n_k$, through:

$$\frac{d}{dt} N(k) = \frac{d}{dk} Q(k) \quad \text{with} \quad Q(k) = 2\pi \int_0^k \mathcal{C}[n_q] q \, dq. \tag{10}$$

As the energy flux, the wave action flux may depend on the wave number and time. Notice that the special writing of

Eqs. (10) may induce the wrong impression that $\int N(k) dk$ is conserved by the dynamics, but this is not so, because $Q(0) \neq Q(\infty)$. Wave turbulence theory predicts a class of exact power-law solutions of the kinetic Eq. (8), found by Zakharov [1], which keep the fluxes constant. More precisely, a (direct) energy cascade is found for which the energy flux P is constant. Similarly, if the wave action is conserved by the dynamics, then an (inverse) wave action cascade corresponding to a constant wave action flux Q can be exhibited. These solutions are named the KZ spectra, because Zakharov's findings are in close relation with the Kolmogorov scaling arguments used in fluid turbulence.

Taking an arbitrary power-law solution, $n_k = A k^{-2x}$, and introducing this into the collisional operator $\mathcal{C}[n_k]$, one readily gets:

$$\mathcal{C}[A k^{-2x}] = A^3 I(x) k^{2-6x}.$$

Here $I(x)$ is a pure function, which depends only on the exponent x and whose expression has been explicitly written in Ref. [8]. Following (9) and (10), the fluxes are then given by:

$$P = A^3 \frac{\pi I(x)}{6(x-1)} k^{6(1-x)} \quad \text{and} \quad Q = A^3 \frac{\pi I(x)}{(2-3x)} k^{4-6x}. \tag{11}$$

Constant energy or wave action fluxes are obtained if the exponents take the values $x = 1$ or $x = 2/3$, respectively. Such arguments guarantee only that the scaling of the solution is consistent with the collisional operator. However, since the denominator vanishes for those exponents, one needs in addition that the collisional operator vanishes in order to obtain stationary solutions of the kinetic equation. This condition is not satisfied for elastic plates, where the inverse cascade of wave action, $x = 2/3$, is not a root of $I(x)$. Only the terms corresponding the $2 \leftrightarrow 2$ resonances vanish for $x = 2/3$, while the terms due to the $3 \leftrightarrow 1$ resonances do not. Then the flux Q formally diverges and the KZ solution is not valid.

On the other hand, $I(x)$ has a double root for $x = 1$ due to a special degeneracy [$I(x)$ vanishes quadratically near $x = 1$, $I(x) \sim (1-x)^2$]. It indicates that both the Rayleigh-Jeans and the KZ solutions exist for $x = 1$. In practice, the resulting flux is zero; thus a logarithmic correction should be included on the final spectrum [8]. Therefore, the above considerations imply that only one cascade is guaranteed, namely a direct cascade of energy toward the small scales, which remarkably is not a simple power law. This KZ spectrum, predicted in Ref. [8], reads (the numerical prefactor is discussed in Ref. [22]):

$$n_k^{\text{direct}} \sim P^{1/3} \frac{\ln^{1/3}(k_*/k)}{k^2}, \tag{12}$$

where P is the energy flux and k_* a cutoff scale. These solutions have been observed in numerical simulations performed with an *ad hoc* dissipation concentrated at small scales only [8,26,27]. However, experimental observations [9,10,28,29] present a slightly different behavior for the direct energy cascade, which is understood as follows. In Ref. [30], it is shown that the dominant low-frequency dissipation rate of the damping suppresses the existence of a window of transparency in the wave-number range probed

by the experiment. It turns out that the stationary spectrum for a vibrating plate comes from the balance among the kinetic collision integral, the forcing, and the damping, displaying no simple KZ scaling spectrum and exhibiting a strong dependence on the damping mechanisms [30].

We conclude this section with the following remark. If one neglects the $3 \leftrightarrow 1$ resonances in the kinetic equation, that is, if one imposes $\mathcal{C}_{13}[n_k] \approx 0$, then an inverse cascade of wave action with constant flux can exist in addition to the direct cascade of energy. This inverse cascade of wave action (from small scales to large scales) reads:

$$n_k^{\text{inverse}} \sim Q^{1/3} \frac{1}{k^{4/3}}, \qquad (13)$$

where $Q < \infty$ is identified as the (constant) wave action flux. This inverse cascade transfers wave action between modes, a self-organization process which may lead to the formation of coherent structures and eventually to the breakdown of the WTT [14,25,31].

The goal of this paper is therefore to investigate the plate dynamics by forcing the vibrations at small scales only in order to observe the genuine transfer of wave action towards large scales despite the presence of the $3 \leftrightarrow 1$ interactions.

III. MANIFESTATION OF AN INVERSE CASCADE

We solve numerically the coupled set of dynamical equations (1, 2) using a pseudospectral method which takes advantage of the linear wave dynamics in Fourier space. Formally, Eqs. (1) and (2) read, in Fourier space:

$$\ddot{\zeta}_{\boldsymbol{k}} = -\omega_k^2 \zeta_{\boldsymbol{k}} + NL_{\boldsymbol{k}} - D_{\boldsymbol{k}} \dot{\zeta}_{\boldsymbol{k}} + I_{\boldsymbol{k}}, \qquad (14)$$

where NL_k stands for the Fourier transform of the nonlinear term including Eq. (2), D_k represents a linear damping, and I_k is the forcing in spectral space. Finally, the temporal integration is performed in the Fourier space using a second-order Adams-Bashford scheme. A standard dealiaising technique for cubic nonlinearity has been tested in previous works [8] with no qualitative changes in the results so no dealiaising is used in the present simulations.

In the present work we use periodic boundary conditions, which are the natural framework to investigate the features of the wave turbulence, the number of modes ranging from 512^2 up to 2048^2, with a mesh size $dx = 1/2$, leading to the spectral ultraviolet cutoff $k_c = \pi/dx = 2\pi$. For numerical stability, the time step used for the simulations is $dt = 0.02$ unit time. To observe the dynamics towards large scale, we force and dissipate the system at small scales only. The dissipation is given by $D_{\boldsymbol{k}} = -\eta(k^2 - k_d^2)H(k - k_d)$, where η is the amplitude of the damping, $H(\cdot)$ is the Heaviside function, and $2\pi/k_d$ is the characteristic scale below which only the dissipation acts. The forcing will be nonzero only in the finite range $[k_i - \delta_i, k_i + \delta_i]$ where

$$I_{\boldsymbol{k}} = A_i \frac{[k^2 - (k_i - \delta_i)^2][(k_i + \delta_i)^2 - k^2]}{k_i^4} e^{i\theta_k(t)}. $$

Here k_i is the characteristic scale of the forcing and δ_i and A_i are its the width and amplitude, respectively. The angular variable $\theta_k(t)$ is a random phase taken in the interval $[0, 2\pi]$, which also changes randomly in time. Notice that this process

injects both energy and wave action around k_i since one cannot separate them formally. To illustrate this inverse transfer mechanism, we take $k_d = k_i + \delta_i$ so the inertial range for an energy cascade vanishes and the low-frequency (large-scale) inverse transparency window is the largest possible available. Finally, we have checked numerically that the results do not depend on the details of the dissipation at small scales.

Although it is required to dissipate the energy at small scales (large k) to reach numerically a stationary state, we have realized distinct numerical simulations with a sink and without it located near $k = 0$, and we conclude that it is not required to absorb nor dissipate the energy (nor the wave action) at the large scale (small k) to reach numerically a stationary state in the time scale of the simulations. This can be explained first by the fact that energy is eventually dissipated at small scales, leading to the general balance between the injected and the dissipated energy. For the wave action, since this quantity is not conserved by the dynamics, everything works as if the wave action is formally absorbed by a sink at $k = 0$ (which is a neutral mode) so there is no need to add such an absorption term near $k = 0$ in the dynamics.

Figure 1 shows the snapshots of the plate deformation at six distinct times of the evolution. Notice the apparent formation of a coherent structure which at the end oscillates at the largest possible mode. This coherent structure appears as a consequence of the long-time evolution which is mostly characterized by the largest modes of oscillation of a plate with small fluctuations.

Figure 2 shows the numerical evolution of the energy and the wave action with time for this numerical simulation. After a transitory regime where both quantities vary, we observe that a quasi-stationary regime is reached above 10^5 unit time approximately.

This dynamics can also be inspected within the evolution of the wave spectrum which is defined following Eqs. (4) and (6) by:

$$n_k(t) = \omega_k \langle |\zeta_{\boldsymbol{k}}|^2 \rangle. \qquad (15)$$

The brackets here stand for a temporal average over the fast time (linear) scale. Therefore it is assumed that the wave system possesses an ergodic-like property, such that temporal and ensemble averages are the same.

Figure 3(a) shows the averaged value of the wave spectrum over the angle in the k space and over a small window of time. The forcing creates a wave action flux towards $k = 0$ that "fills" the spectrum at large scale. This can be observed on Fig. 3(b), which presents the wave action flux (10) at different times, computed explicitly as a sum over discrete modes $Q(k) = 2\pi \sum_{q=0}^{k} k \, \partial_t n_k$. [Note that, by definition, $Q(0) = 0$.] For large times (again, above 10^5 time units) the spectrum tends asymptotically to a stationary form that exhibits a power law with an exponent surprisingly close to the hypothetical 4/3 inverse cascade exponent (13) which is forbidden by the $3 \leftrightarrow 1$ interactions. Similarly, the wave action flux Q converges to an almost constant value. Notice, however, that the dynamics is not steady but only in a "quasi"-stationary regime since the large-scale modes still exhibit a slow dynamics.

In the following, we will show that the evolution of this amplitude spectra can be decomposed in two distinct regimes
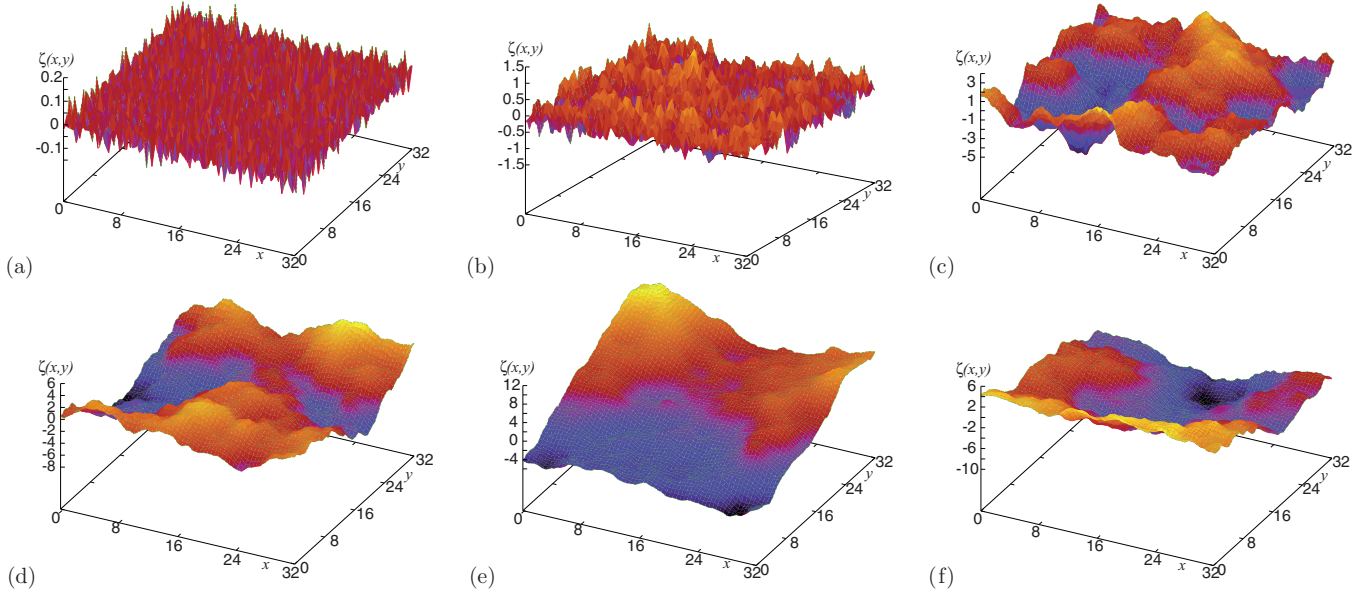
FIG. 1. (Color online) Snapshots of the out-of-plate displacement $\zeta(x,y,t)$ obtained by the numerical simulation of the Föppl–von Kármán equations (1) and (2) at six different times: (a) $t = 22 \times 10^3$, (b) $t = 50 \times 10^3$, (c) $t = 62 \times 10^3$, (d) $t = 82 \times 10^3$, (e) $t = 162 \times 10^3$, and (f) $t = 202 \times 10^3$. The injection is made at small scales, with $k_i = 4.5$ and $\delta_i = 0.5$. Numerical dissipation acts at smaller scale, starting at the end of the injection range ($k_d = 5$). The amplitude of the injection is $A_i = 0.0001$. The system size is 1024^2 units with 2048^2 modes and $k_c = 2\pi$. Note that the vertical scales differ from one figure to the other, growing from (a) to (f). Despite this change of scale, the amplitude of the small spatial scales can always be observed. Notice the formation of a large-scale structure as time increases.

in time, both being dominated by weakly random waves. The first regime displays a self-similar behavior corresponding to a nonconstant wave action flux. On the other hand, the latter regime displays a quasisteady behavior consistent with an inverse cascade with a nearly $k^{-4/3}$ spectrum. This regime exhibits an almost constant flux of wave action towards the large scales [see Fig. 3(b)] except precisely near the largest scale of the system ($k \approx 0$).

IV. SIGNATURE OF A FINITE-TIME SINGULARITY

The first stage of the evolution appears as the formation in time of a spectrum characterized by a nonuniform flux of wave action from the short to the long scales, as shown in Fig. 3. This flux fills the spectrum from the large k towards small k, tending

to a steady power-law spectrum with an almost constant flux of wave action Q [Fig. 3(b)].

It is important to notice that this built-in time spectrum is of finite capacity [32], that is, $\int_0^k n_k d^2k < \infty$ (taking $n_k \propto k^{-\alpha}$ with $\alpha \sim 4/3$). Therefore, one expects, assuming a constant injection of wave action in the injecting domain around k_i, the formation of such a spectrum in finite time. This situation is in fact similar to the self-similar formation of a condensate of weakly classical nonlinear waves [11,12,14,31] and we shall characterize quantitatively this self-similar dynamics. To do that, we compute the characteristic length scale involved in the self-similar process via the negative moments (typically $n \leqslant -2$ later) of the spectral distribution [1]:

$$\langle k^n \rangle = \left[\int k^n n_k(t) \, d^2k \right] \Big/ \left[\int n_k(t) \, d^2k \right]. \qquad (16)$$
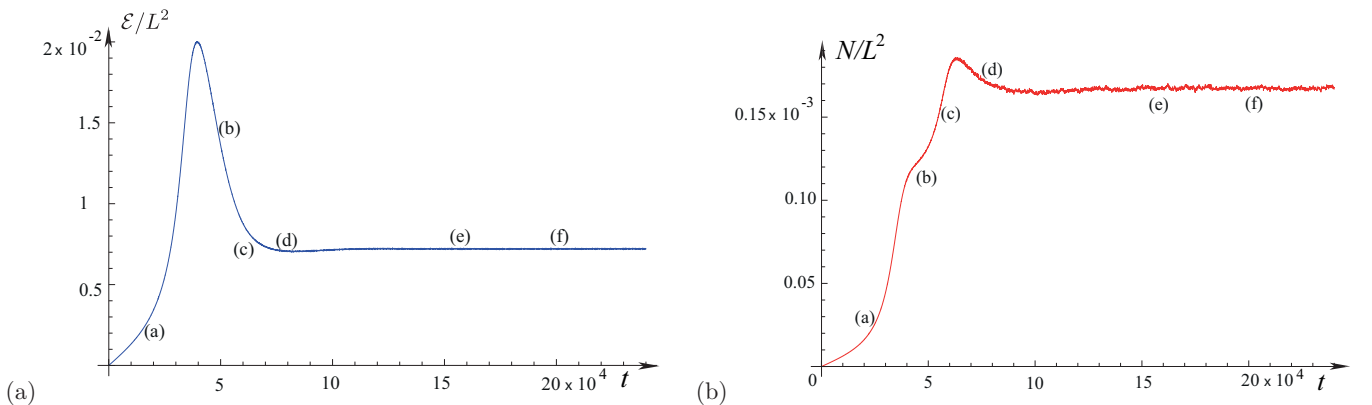
FIG. 2. (Color online) (a) Evolution of the energy density $\mathcal{E}/L^2$ and (b) the wave action density $\mathcal{N}/L^2$ with time. The parameters are the same than those of Fig. 1. The time of the different snapshots of Fig. 1 are indicated on the curves.
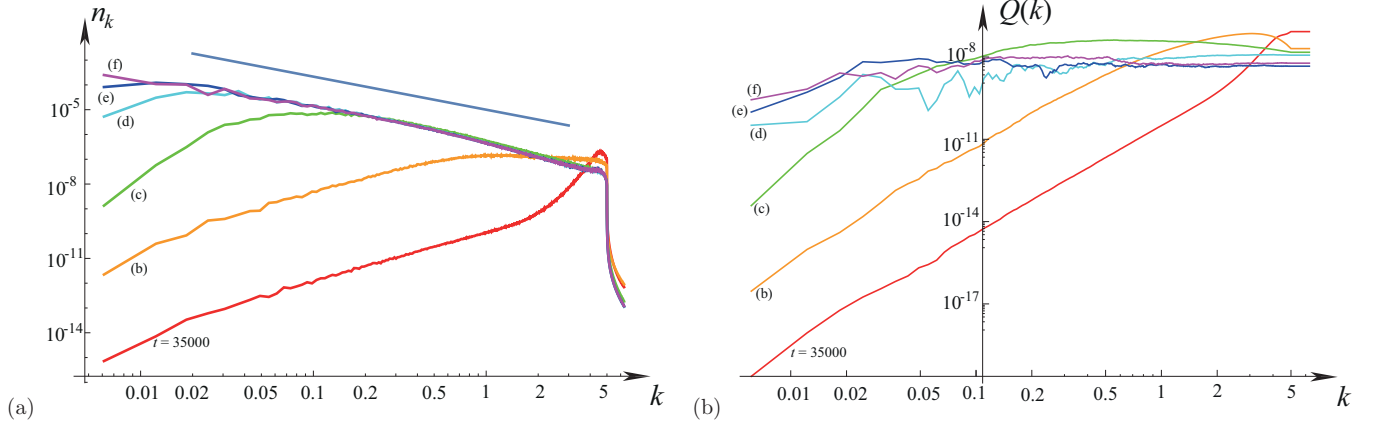
FIG. 3. (Color online) (a) Angular average of the spectra, n_k, as a function of wave number k in log-log scale, at different time steps starting at $t = 35 \times 10^3$. Subsequent spectra are labeled according to the snapshots of Fig. 1. The straight line indicates a power law $k^{-4/3}$ as a reference guide. (b) Under the same conditions log-log plot of the wave action flux $Q(k,t)$ as a function of wave number for the same times.

This allows us to define characteristic wave numbers of the spectrum through $\langle k^n \rangle^{1/n}$. Figure 4 shows these characteristic wave number to the power 2/3 computed numerically for different moments from $n = -2$ to $n = -7$ at short times ($t < 80\,000$ time units). We observe that the different curves exhibit a linear decrease below a critical time t_*, suggesting the singular behavior for the critical wave number of the spectrum:

$$k_0(t) \sim (t_* - t)^{3/2}, \quad \text{with} \quad t_* \approx 65\,000. \quad (17)$$

It is the signature of a finite time singularity that would be present if the asymptotic spectrum would be filled with a constant wave action flux.
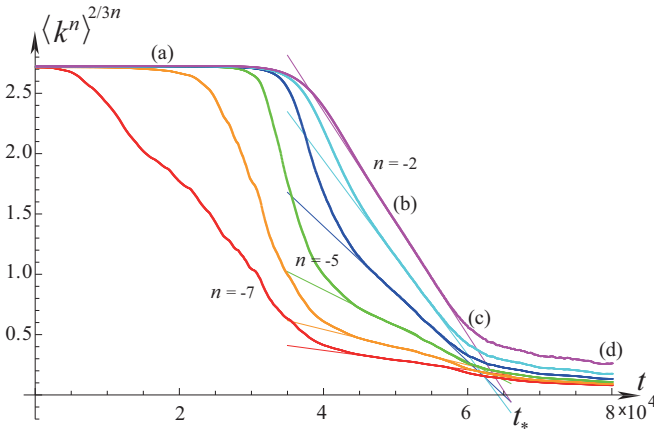
FIG. 4. (Color online) The evolution of the characteristic wave number $[k_0(t)]^{2/3}$ computed through the n-th moments of the distribution (16) for consecutive n ranging from $n = -7$ up to $n = -2$ (labeled explicitly on the figure). The simulation conditions are as for other figures. The straight lines correspond to a linear fit $K_n(t_* - t)$. Notice that almost all moments vanish near an unique critical time. The corresponding values for this time are $t_* = 85971.8$ for $n = -7$, $t_* = 76\,926.9$ for $n = -6$, $t_* = 69\,154.8$ for $n = -5$, $t_* = 64\,971.5$ for $n = -4$, $t_* = 64\,173.4$ for $n = -3$, $t_* = 65\,376.9$ for $n = -2$. Despite the inaccuracy of the higher-order moments $(-7, -6)$ all other critical times are around $t_* \approx 65\,000$, indicating the independence of t_* with order n (notice that the range of the temporal axis is different from the one of Figs. 2 and 7).

This singular behavior suggests a self-similar solution of the form [11,12]:

$$n_k(t) = \frac{1}{(t_* - t)^\alpha} \phi \left[\frac{k}{(t_* - t)^\beta}, \log(t_* - t) \right]. \quad (18)$$

From relation (17), we obtain $\beta = 3/2$. The parameter α is settled assuming that wave turbulence theory is valid, so the self-similar solution (18) should obey the kinetic equation (8); $\alpha = 2$ is then the only possible choice to balance the left-hand side and the right-hand side terms in the kinetic equation (8). Finally, the function ϕ satisfies an autonomous equation, which reads:

$$\frac{\partial}{\partial \tau} \phi(s, \tau) = \left[2\phi(s, \tau) + \frac{3}{2} s \frac{\partial}{\partial s} \phi(s, \tau) \right] - \mathcal{C}[\phi(s, \tau)], \quad (19)$$

where $s = k(t_* - t)^{-3/2}$ is the self-similar variable, $\tau = \log(t_* - t)$, and $\mathcal{C}$ is formally the same collisional operator of (8) but with the scaling variable s instead of k.

Thus the self-similar function $\phi(s, \tau)$ follows an integrodifferential equation (19), with the boundary condition at the origin, $\phi(0, \tau) = 0$, and with the asymptotic behavior

$$\phi(s, \tau) = \frac{1}{s^{2\nu}} e^{\lambda \tau} \quad (20)$$

for $s \to \infty$ and $\tau \to -\infty$ ($t \to t_*$). The condition $\lambda = 2 - 3\nu$ ensures that, in this limit, the tail of the spectrum does not depend on time, as it is observed in Fig. 5. Notice that one can always rescale ϕ of the nonlinear equation (19) to settle the pre factor in (20) to unity.

Equation (19) represents in fact a nonlinear eigenvalue problem for ν, which indicates the power law of the self-similar spectrum at large wave number. Such problems are difficult to solve analytically and even numerically since no systematic approaches exist [11,12]. Here we will develop an indirect method providing an approximate value only for ν.

Using the relation between the theoretical values of $\alpha = 2$ and $\beta = 3/2$, we can rescale the spectra at different times following the self-similar formula (18) by plotting $k_0(t)^{4/3} n_k(t)$ as a function of $s = k/k_0(t)$ taking $k_0(t) = \langle k^{-2} \rangle^{-1/2}$. A good collapse of the spectra into a single universal curve is then observed in Fig. 5, particularly at large wave number s.
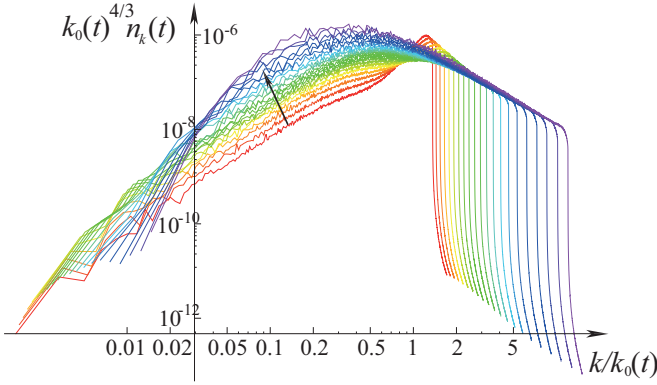
FIG. 5. (Color online) Plot (log-log scale) of the rescaled spectra $k_0(t)^{4/3}n_k(t)$ as function of the rescaled variable $s = k/k_0(t)$, with $k_0(t) = \langle k^{-2}\rangle^{-1/2}$. This choice shows a very good collapse of all curves in the large k limit. The spectra plotted correspond to times ranging from $t = 40\,000$ up to $t = 60\,000$ units (the arrow denotes the time direction).

In fact, the envelope of all the rescaled curves defines the function

$$\phi_\infty(s) = \lim_{\tau \to -\infty} \phi(s,\tau).$$

Averaging the curves near t_* for the same simulations but with different system sizes $L = 256$, $L = 512$, and $L = 1024$, we obtain a single curve with better resolution for $\phi_\infty(s)$, as shown on Fig. 6(a). Then, seeking the exponent ν such that $s^{2\nu}\phi_\infty(s) \to 1$ for large s, the best fit gives $\nu \approx 0.873$, which significantly differs (higher) from the theoretical value $\nu = 2/3$ of the inverse cascade Eq. (13). Let us emphasize that it is in fact consistent with such unsteady regime which fills the spectrum from small to large scales.

The particular shape of the universal function $\phi_\infty(s)$ requires a few comments. First, the spectrum decreases near $s = 0$, in agreement with the boundary condition $\phi(0,\tau) = 0$. Second, as expected, in the self-similar variables the forcing position in the spectrum tends to $s \to \infty$, as one approaches the singularity, therefore the forcing only acts as a boundary
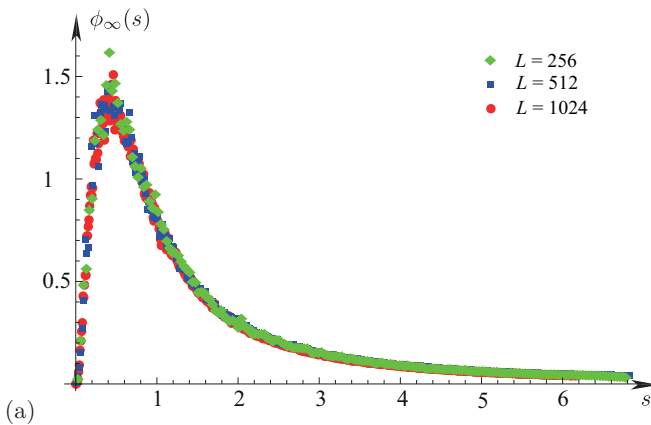
condition in the ultraviolet regime. Finally, the matching region between the inner and outer behavior corresponds to the maximum of the function.

V. VALIDITY OF WAVE TURBULENCE AND THE LATE STAGE REGIME

The self-similar behavior (18), discussed in the previous section, predicts that wave turbulence assumptions will not be valid near the finite singularity. In general, wave turbulence theory is no longer valid either because high amplitudes of the spectrum are reached at large scale or because of the discrete dynamics of the modes corresponding to wave lengths close to the size of the computational domain.

The nonlinear transition due to high amplitude will appear at small k when, for some wave numbers, the nonlinear time scale deduced from Eq. (8) is of the same order as the period of the linear wave [32]. In the present case of (18) one has that the nonlinear and the linear frequencies scale respectively as:

$$\omega_{\mathrm{NL}}(k) \sim \frac{1}{n_k}\frac{dn_k}{dt} \sim \frac{1}{t_* - t} \quad \text{and} \quad \omega_k \sim (t_* - t)^3 \quad (21)$$

near t_*. Therefore one expects the nonlinearities to be large as $t \to t_*$ so WWT cannot be applied anymore.

In the following we compute numerically two distinct criteria to quantify the ratio between nonlinear and linear contributions. First, we computed the ratio between the nonlinear energy, $E_4 = -\int[\frac{1}{2}(\Delta\chi)^2 + \frac{1}{2}\chi\{\zeta,\zeta\}]dxdy$ and the linear energy $E_2 = \int[\frac{1}{2}(\partial_t\zeta)^2 + \frac{1}{8}(\Delta\zeta)^2]dxdy$, already discussed in (3). This is a global criteria which depends only on time and indicates the relative importance of both energies in the dynamics. Figure 7(a) shows this ratio as a function of time. It is observed that E_4/E_2 is at most of the order of 6×10^{-3}, indicating that the nonlinear contributions (the stretching contributions) to the energy are really small. Incidentally, the maximum of E_4/E_2 arises for $t \approx t_*$, confirming the existence of a precursor to a singularity. This can be understood by the following scaling argument: near the singularity, the quadratic energy would scale like $E_2 \sim \int \omega_k n_k \, d^2k \sim (t_* - t)^4$, while
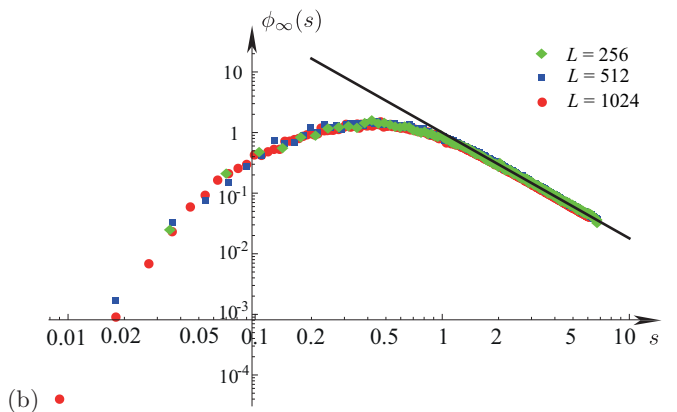
FIG. 6. (Color online) (a) Self-similar universal function $\phi_\infty(s)$ as a function of the self-similar variable, s, in linear scale. The data come from the same conditions as Fig. 3 but for three distinct system sizes: $L = 256$, $L = 512$, and $L = 1024$, as indicated in the figure. (b) The same self-similar universal function but in log-log scale. Fitting the exponent ν such that $s^{2\nu}\phi_\infty(s) \to 1$ for large s provides $\nu \approx 0.873$, which is slightly larger than $2/3$.
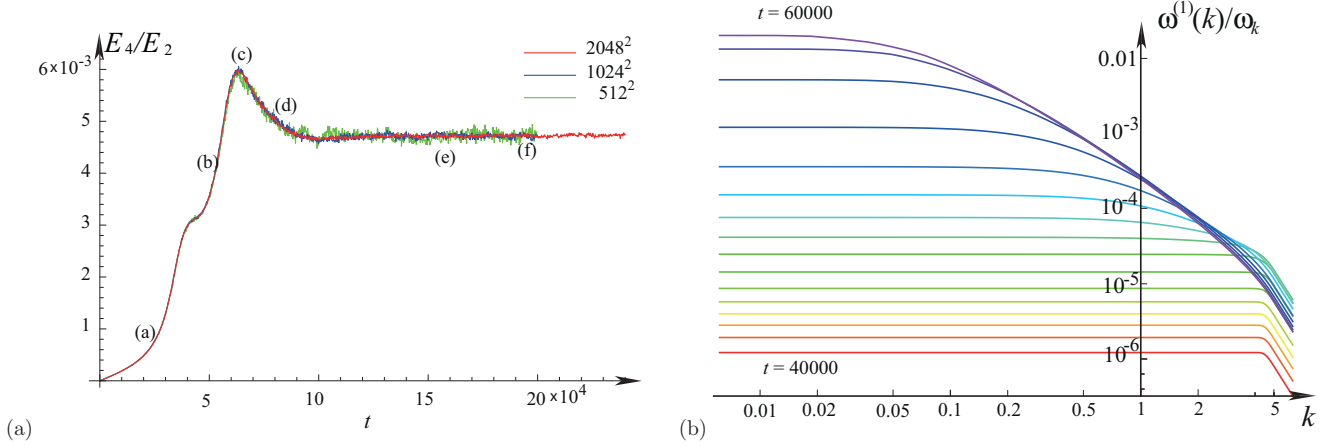
FIG. 7. (Color online) (a) The ratio E_4/E_2 vs t, under the same conditions as in Fig. 3 but for three distinct system sizes $L = 256$, 512, and 1024 with 512^2, 1024^2, and 2048^2 modes, respectively. (b) The ratio $\omega^{(1)}(k)/\omega_k$ as a function of the wave number k for different times steps in log-log scale. The range of time plotted corresponds exactly to the one used in Fig. 5, that is, from $t = 40\,000$ time units up to $t = 60\,000$. Both quantities show the weakness of the nonlinearities in all wave numbers and at all times, justifying the validity of the weak turbulence theory.

the fourth-order energy (the stretching) would follow $E_4 \sim \int n_k^2 \, d^2k \sim 1/(t_* - t)$, hence $E_4/E_2 \sim (t_* - t)^{-5}$.

Although this criterium suggests that the nonlinear behavior is globally weak, one cannot ensure that the nonlinearities are uniformly weak and in particular that the nonlinearities are effectively small for all scales. A local (in k) criteria can be used numerically via the ratio between the linear time scale and the first-order nonlinear correction to the frequency (7), as stated in Eq. (21).

Figure 7(b) plots the ratio $\omega^{(1)}(k)/\omega_k$, from (7), as a function of the wave number at different times. One notices that the infrared behavior of the quotient $\omega^{(1)}(k)/\omega_k$ increases significantly when approaching the singularity. Nevertheless, it is always less than 10^{-2}, which implies that the weak amplitude expansion is presumably uniformly valid, even near the singularity signature.

Though wave turbulence theory predicts breakdown of the theory (21), because $\omega_{\mathrm{NL}}(k)/\omega_k \sim (t_* - t)^{-4}$, one observes that direct numerical simulations on the Föppl–von Kármán equations (1) and (2) do not allow the nonlinearities to be of the order of unity. Nevertheless, in the case of a large forcing, such effects have been seen in our numerics and it could be then a reason for the breakdown of wave turbulence.

In conclusion, in the limit of small forcing investigated here, the system does not create strong nonlinearities although the singular behavior is cured near t_*. This effect comes from the discrete properties of the system which becomes relevant at this stage, in particular, to the discrete dynamics of the first modes of the plate (the lowest in term of frequency) which have to be considered in a modified picture of wave turbulence theory [16,33].

VI. DISCUSSION

Our numerical study reveals that a time-dependent wave action inverse cascade is built in time and eventually reaches the infrared region in finite time through a clearly identifiable self-similar process. In this early time regime, the wave system is driven by the WWT kinetic equation (8), and the

dynamics is characterized by a self-similar evolution which should eventually blow up in finite time. However, near the singularity, the dynamics is smoothed and the kinetic equation is no longer valid: In the small forcing cases, investigated here, the system is governed by the discrete dynamics of the largest modes coupled with the continuous spectrum (a discrete breakdown). On the other hand, for larger forcing (not studied here), a regularization of the dynamics through the nonlinear breakdown of the WWT is expected (nonlinear breakdown).

For other systems where the wave action is a conserved quantity (for instance, for the nonlinear Schrödingier equation), a condensate at (or around) $k = 0$ forms, changing the post blow-up dynamics [14,31]. Such effects are not possible here since the wave action is not conserved by the dynamics. The mode $k = 0$ is neutral and remains null with time. Nevertheless, as it has been shown for the nonlinear Schrödinger equation [34], the first modes of the systems can exhibit an autonomous dynamics. Figure 8(a) shows precisely the evolution with time of the amplitude for the lowest mode of the plates: After the blow-up time t^*, the amplitude of this mode grows more or less linearly in time but also exhibits important oscillations. Finally, for these large times, a stationary regime is eventually reached where the spectrum behaves approximatively like $n_k \sim 1/k^{4/3}$ for the low wave numbers [$k < 0.2$ in Fig. 8(b)] and $n_k \sim 1/k^{2\times0.873}$ for the smaller wavelength [$0.5 < k < k_d$ in Fig. 8(b)]. This stationary regime is not surprising, since we expect that the long-time behavior does not change the power law built by the self-similar evolution (Sec. III), and long wave modulations transfer wave action toward $k = 0$ with precisely the Kolmogorov-Zakharov spectrum, $n_k \sim 1/k^{4/3}$, which corresponds to the constant wave action flux solution found for $\mathcal{C}_{22}[n_k]$. However, notice that this regime is not formally steady for the smallest wave numbers, where the dynamics appears rather more like a relaxation towards a full stationary dynamics.

In conclusion, although an elastic vibrating plate does not formally posses a wave action conservation law, an undoubtedly inverse cascade of wave action is observed, exhibiting a complex time-dependent dynamics. The process
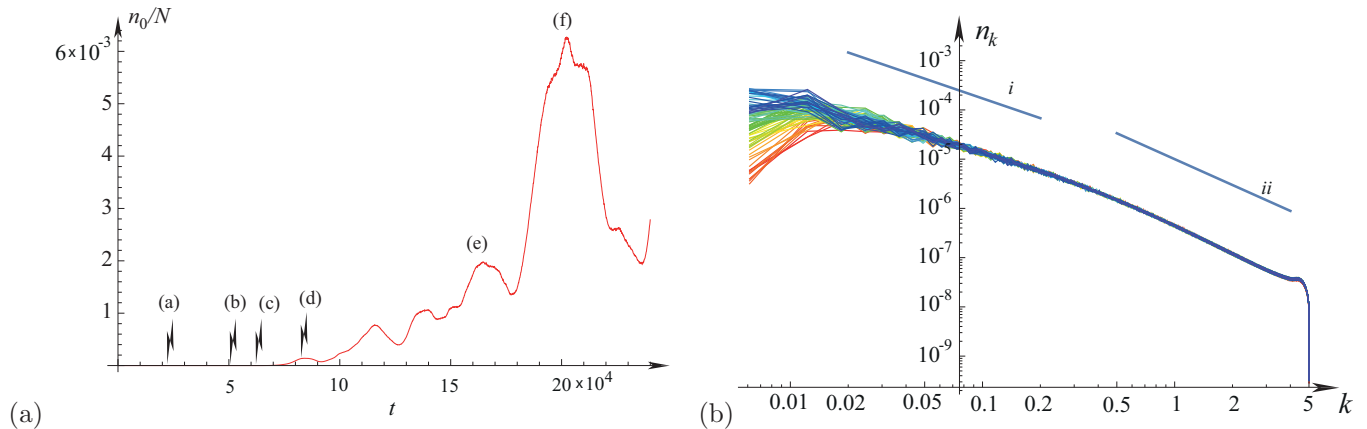
FIG. 8. (Color online) (a) Evolution of the fraction of the first mode. This plot corresponds exactly to the numerical simulation of Fig. 1 and the times of the different snapshots are indicated. (b) The long-time evolution of the spectra. The time considered are from $t = 80\,000$ units up to $t = 240\,000$. The spectra only vary for the small wave numbers where it relaxes towards the stationary power-law spectrum $n_k \propto k^{-2\nu}$ with $\nu \sim 2/3$. The line (*i*) correspond to a 4/3 power law, while the line (*ii*) corresponds to a 2×0.873 power law which represents better the behavior in the large k limit.

of formation of such an inverse cascade is ruled by a self-similar evolution of the spectra which transfers wave action from short-wavelength scales up to long-wavelength scales. Formally, the observed self-similar solution blows up, leading to a singular behavior which is cured in the original system, probably because of the finite size of the system and the role played by the discreteness of the modes. The late evolution of the system is also governed by wave turbulence theory, although the discrete nature of the lowest modes modifies the overall picture. This scenario is consistent with the formation of a coherent structure which is characterized by the largest modes of oscillation [see Fig. 7(a)] plus small fluctuations.

Remarkably, the nonlinear fraction of the energy indicates that this coherent structure makes the stretching very small.

[1] V. E. Zakharov, V. S. L'vov, and G. Falkovich, *Kolmogorov Spectra of Turbulence I* (Springer, Berlin, 1992).

[2] S. Nazarenko, *Wave Turbulence* (Springer, Berlin, 2011).

[3] A. C. Newell and B. Rumpf, Annu. Rev. Fluid Mech. **43**, 59 (2011).

[4] E. Falcon, C. Laroche, and S. Fauve, Phys. Rev. Lett. **98**, 094503 (2007).

[5] G. Düring and C. Falcón, Phys. Rev. Lett. **103**, 174503 (2009).

[6] A. I. Dyachenko, A. O. Korotkevich, and V. E. Zakharov, Phys. Rev. Lett. **92**, 134501 (2004).

[7] S. Lukaschuk, S. Nazarenko, S. McLelland, and P. Denissenko, Phys. Rev. Lett. **103**, 044501 (2009).

[8] G. Düring, C. Josserand, and S. Rica, Phys. Rev. Lett. **97**, 025503 (2006).

[9] A. Boudaoud, O. Cadot, B. Odille, and C. Touzé, Phys. Rev. Lett. **100**, 234504 (2008).

[10] N. Mordant, Phys. Rev. Lett. **100**, 234505 (2008).

[11] R. Lacaze, P. Lallemand, Y. Pomeau, and S. Rica, Physica D **152–153**, 779 (2001).

[12] C. Josserand, Y. Pomeau, and S. Rica, J. Low Temp. Phys. **145**, 231 (2006).

[13] N. G. Berloff and B. V. Svistunov, Phys. Rev. A **66**, 013603 (2002).

[14] C. Connaughton, C. Josserand, A. Picozzi, Y. Pomeau, and S. Rica, Phys. Rev. Lett. **95**, 263901 (2005).

[15] R. H. Kraichnan, Phys. Fluids **10**, 1417 (1967).

[16] S. Y. Annenkov and V. I. Shrira, Phys. Rev. Lett. **96**, 204501 (2006).

[17] A. O. Korotkevich, Phys. Rev. Lett. **101**, 074504 (2008).

[18] G. E. Falkovich and A. V. Shafarenko, J. Nonlinear Sci. **1**, 457 (1991).

[19] C. Connaughton, A. C. Newell, and Y. Pomeau, Physica D **184**, 64 (2003).

[20] L. Deike, M. Berhanu, and E. Falcon, Phys. Rev. E **85**, 066311 (2012).

[21] L. D. Landau and E. M. Lifshitz, *Theory of Elasticity* (Pergamon Press, New York, 1959).

[22] G. Düring, C. Josserand, and S. Rica (unpublished).

[23] N. Yokoyama and M. Takaoka, Phys. Rev. E **89**, 012909 (2014).

[24] V. E. Zakharov and N. N. Filonenko, Dokl. Akad. Nauk SSSR **170**, 1292 (1966) [Sov. Phys. Dokl. **11**, 881 (1967)].

[25] S. Dyachenko *et al.*, Physica D **57**, 96 (1992).

[26] N. Yokoyama and M. Takaoka, Phys. Rev. Lett. **110**, 105501 (2013).

[27] B. Miquel, A. Alexakis, C. Josserand, and N. Mordant, Phys. Rev. Lett. **111**, 054302 (2013).

[28] P. Cobelli, P. Petitjeans, A. Maurel, V. Pagneux, and N. Mordant, Phys. Rev. Lett. **103**, 204301 (2009).

[29] B. Miquel and N. Mordant, Phys. Rev. Lett. **107**, 034501 (2011).

[30] T. Humbert, O. Cadot, G. Düring, C. Josserand, S. Rica, and C. Touzé, Euro. Phys. Lett. **102**, 30002 (2013).

[31] G. Düring, A. Picozzi, and S. Rica, Physica D **238**, 1524 (2009).

[32] A. Newell, S. Nazarenko, and L. Biven, Physica D **152–153**, 520 (2001).

[33] E. Kartashova, *Nonlinear Resonance Analysis* (Cambridge University Press, Cambridge, UK, 2010).

[34] P. Miller, N. Vladimirova, and G. Falkovich, Phys. Rev. E **87**, 065202 (2013).